Biomass-derived carbons physically activated in one or two steps for CH_4/CO_2 separation

Gianluca Greco [a, *], Rafael L.S. Canevesi [b], Christian Di Stasi [a], Alain Celzard [b], Vanessa Fierro [b], Joan J. Manyà [a, **]

[a] *Aragon Institute of Engineering Research (I3A), Thermochemical Processes Group, University of Zaragoza, Escuela Politécnica Superior, crta. Cuarte s/n, Huesca, E-22071, Spain*
[b] *Université de Lorraine, CNRS, IJL, Épinal, F-88000, France*

ABSTRACT

The present study aims at evaluating the suitability of producing activated carbons (ACs) derived from wheat straw by a one-step synthesis approach, as an alternative to more conventional two steps production processes (i.e., pyrolysis and subsequent activation). The performance of the produced ACs, in one or two steps, as sustainable and selective CO_2 adsorbents for CH_4/CO_2 separation is compared. In addition, the influence of pyrolysis conditions on the properties of the resulting two-step ACs is carefully analyzed. We show that the biochar-based precursors of ACs presenting the best textural properties were obtained under mild conditions of maximum temperature and absolute pressure during pyrolysis. The one-step ACs were fully comparable —in terms of textural properties as well as CO_2 uptake and selectivity— to those produced by the more conventional two-step synthesis process. In addition, results obtained from breakthrough curve simulations highlight that the best AC in terms of CH_4 recovery under dynamic conditions was produced by a one-step activation. Therefore, the one-step process appears to be as an attractive route for the production of engineered carbon materials, which can lead to significant cost savings in large-scale production systems.

© 2022 The Authors. Published by Elsevier Ltd. This is an open access article under the CC BY-NC-ND license (http://creativecommons.org/licenses/by-nc-nd/4.0/).

1. Introduction

Serious concerns about climate change and the growing global energy demand have led to a great interest in renewable energies [1]. One of the most attractive options is to use biofuels as a valuable alternative to widely used fossil fuels. Having a low environmental impact, biofuels could contribute significantly to the reduction of hydrocarbons, SO_x and CO_2 emissions [2]. Biogas, mainly produced by anaerobic digestion processes [3], can certainly be considered as a biofuel, due to its significant methane content. Before being used as a biofuel, biogas needs to be refined by reducing its CO_2 content, in order to increase its heating value and bring it closer to that of natural gas [4], and to reduce the risk of pipeline corrosion in presence of water [5].

The most commonly used technologies for CO_2 separation are chemical absorption into aqueous amine blended solutions [6], multistage membrane separation using polymeric materials [7],

and adsorption into porous materials in fixed beds [8]. The former is considered the current benchmark technology, thanks to its level of maturity reached after sixty years [9]. However, the main drawback of this technology is the energy penalty associated with the regeneration step [10]. Adsorption in porous solids appears as an emerging alternative for CO_2 separation, due to its relatively low cost and high energy efficiency [11]. As potential adsorbents for large-scale systems, activated carbons (ACs) has attracted increasing interest in the last years, due to their relatively high CO_2 adsorption capacity (over 2 mol kg^{-1} at ambient conditions [12–14]), fast kinetics, thermal stability, chemical resistance and relatively low costs (for production and regeneration) compared to other adsorbents such as zeolites and metal organic frameworks (MOFs) [5,15,16]. When used in biogas upgrading applications, ideal ACs should exhibit high selectivity towards CO_2, guaranteed by appropriate pore size distribution (PSD) and surface chemistry [17]. However, designing adsorbents based on kinetics could be very complex, as CO_2 and CH_4 molecules have very similar kinetic diameters (0.34 and 0.38 nm, respectively) [16]. On the other hand, CO_2 is a polar molecule with a quadrupole moment of 13.4

* Corresponding author.
** Corresponding author.
E-mail addresses: greco@unizar.es (G. Greco), joanjoma@unizar.es (J.J. Manyà).

10^{-40} cm^2, whereas CH$_4$ is non-polar. This significant difference in polarity makes the presence of polar functional groups on the adsorbent surface very useful to increase the CO$_2$ selectivity [18] to values higher than 8 [19,20].

Biomass is a sustainable way to produce ACs. In general, the process consists of two main steps: pyrolysis and subsequent activation. The former involves the thermal degradation of biomass, resulting in a solid carbon precursor known as biochar. Given the large number of variables influencing the pyrolysis process and the wide variety of biomass sources, there are significant differences in the final biochar properties [21,22]. With this in mind, optimization of pyrolysis conditions is necessary to obtain the most suitable biochar for its subsequent activation into porous carbon materials. Since pristine biochar typically has a low specific surface area (SSA) and a porous texture consisting mainly of narrow micropores [23], a secondary activation step (physical or chemical [24,25]) is required to accomplish further porosity development.

As an alternative to the two-step production process mentioned above, biomass-derived ACs can also be synthesized by a one-step thermochemical process. For this purpose, the highest pyrolysis temperature has to be raised to more than 650 °C and the inert gas atmosphere (usually N$_2$) has to be replaced by an atmosphere containing an activating agent (e.g., CO$_2$, H$_2$ or H$_2$O). This process is considered a very interesting solution in terms of energy recovery, especially for large-scale production systems. The results of the relatively few published studies on the production of ACs from biomass by a one-step process [26–29] are certainly encouraging, since similar or even better properties have been reported for ACs produced in one step compared to traditional ACs produced in two steps. For instance, González et al. [29], who produced olive stones-derived ACs by one-step physical activation (with CO$_2$ at 800 °C), reported excellent CO$_2$ uptakes (1.75 mmol g^{-1} at 35 kPa and 25 °C). Bergna et al. [30] carried out a study based on the comparison between one-step and two-step production pathways, observing that ACs produced through one-step activation generally had higher surface areas as well as higher total pore volumes. In the same study, the authors reported that the final carbon yield was higher when ACs where prepared by two-step process, whereas no significant differences were detected in the total carbon content between the two types of activation.

In view of all the above, the aim of the present study is to contribute to fill the gaps that still exist in establishing the most suitable route for the conversion of biomass feedstock into ACs with tuned porosity. To this end, a systematic and parametric study of the effects of several pyrolysis conditions (maximum temperature, absolute pressure, gas residence time, and type of pyrolysis atmosphere) on the textural properties of the resulting wheat-straw-derived ACs —produced via pyrolysis and subsequent physical activation with CO$_2$ at 800 °C— was performed. In addition, several wheat straw-derived ACs were prepared through a one-step process under different operating conditions (maximum temperature, absolute pressure and CO$_2$ content in the carrier gas). The most promising ACs (i.e., those with the best textural properties for CO$_2$ adsorption from both one-step and two-step conversion processes) were then tested as selective adsorbents for CO$_2$/CH$_4$ separation.

2. Materials and methods

2.1. Biomass feedstock

The wheat straw (WS) pellets (7 mm OD and approximately 12 mm long, with an apparent density of 400 kg m^{-3}) used as feedstock in this work were described elsewhere [31,32]. Demonstrating the real potential of WS pellets in biogas upgrading would be of great importance in terms of circular economy for this abundant,

autochthonous resource in Aragon (Spain), which represents a significant share of local agricultural disposals. The as-received biomass was directly pyrolyzed without any preliminary milling step in order to maximize the final carbonization efficiency [33,34]. WS pellets were characterized by proximate analysis (according to ASTM standards for moisture, ash, and volatiles), and X-Ray Fluorescence (XRF) spectroscopy analysis (ADVANT'XP + XRF spectrometer from Thermo ARL, Switzerland) to determine inorganic constituents. The contents of hemicelluloses, cellulose and lignin were determined following an analytical approach described previously [32].

2.2. One-step activation

The one-step activation process was performed using the same bench-scale fixed-bed reactor described in previous works [31,32]. The following ranges of operating conditions were considered: maximum temperature between 650 and 750 °C, absolute pressure between 0.2 and 0.9 MPa, reactor environment varying between pure N$_2$ and a binary CO$_2$/N$_2$ mixture (75:25 v/v), and constant gas residence time of 100 s. In order to study the pyrolysis behavior in this range of process parameters, experiments using a pure N$_2$ atmosphere were included in the experimental design (see Fig. 1). The heating rate and the dwell time (at the maximum temperature) were 5 °C min^{-1} and 1 h, respectively.

2.3. Two-step activation

The pyrolysis step was performed using the same bench-scale fixed-bed reactor as for the one-step activation. The maximum temperature, absolute pressure, and gas residence time varied in the range of 400–550 °C, 0.2–0.9 MPa, and 100–200 s, respectively. In addition, the pyrolysis atmosphere adopted for these experiments varied from pure N$_2$ to a CO$_2$/N$_2$ mixture (60:40 v/v). As before, the heating rate and the dwell time (at the maximum temperature) were 5 °C min^{-1} and 1 h, respectively. More details on the pyrolysis setup are available in Appendix A (see Fig. A1). The resulting material from pyrolysis step is called biochar (see Fig. 1).

All biochars obtained after pyrolysis were then physically activated at 800 °C and atmospheric pressure under a pure CO$_2$ atmosphere. The device used for activation [35] consisted of a tubular reactor (Inconel 600 alloy, 600 mm long and 28 mm ID), placed inside a vertical tubular furnace (model EVA 12/300 mm from Carbolite Gero, UK). A K-type thermocouple was placed along the longitudinal axis of the reactor to monitor the temperature inside the bed in real-time. Following the same procedure as in a previous work [35], the raw biochars were first ground and sieved to obtain particle sizes between 0.21 and 1.41 mm. Then, samples of 10 g were heated at 10 °C min^{-1} under a constant flow of N$_2$. Once the activation temperature was reached (i.e., 800 °C), the gas feed was switched from N$_2$ to CO$_2$ and held isothermally for 1 h. Under these conditions, the gas-hourly space velocity (GHSV) was approximately 7000 h^{-1}. Fig. 1 summarizes the production process pathways and the range of operating conditions adopted in this study.

2.4. Characterization of activated carbons

The degree of burn-off (X_i) was estimated as follows:

$$X_{1S} = (m_{biomass} - m_f)/m_{biomass} \cdot 100 \quad (1)$$

$$X_{2S} = (m_{biochar} - m_f)/m_{biochar} \cdot 100 \quad (2)$$

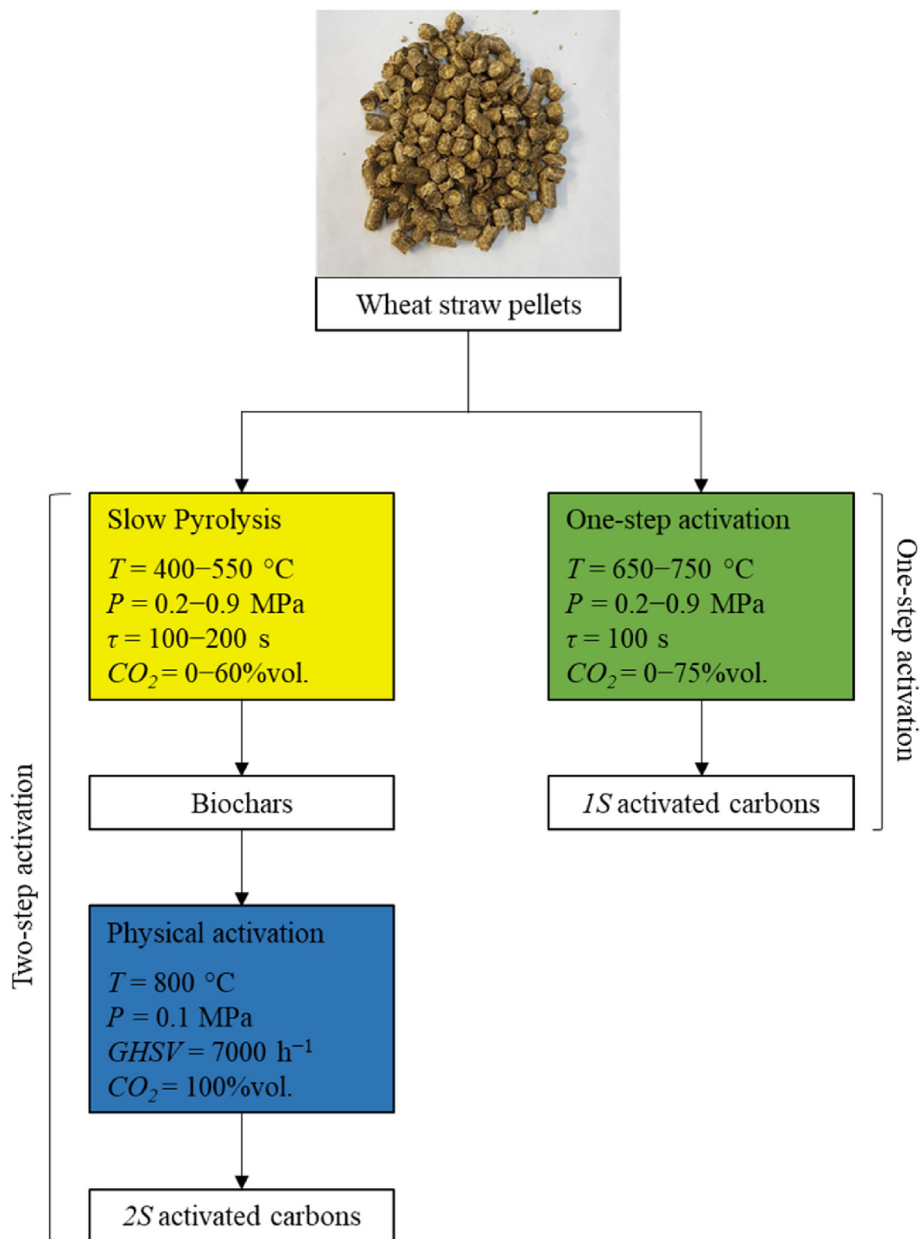where i refers to the type of activation process: one-step (1S) or

Fig. 1. Overview of the production pathways for one-step (1S) and two-step (2S) activated carbons.

two-step (*2S*). $m_{biomass}$, $m_{biochar}$, and m_f are the masses of biomass, biochar and final sample, respectively. It is important to note that, unlike the burn-off of *2S* activated carbons (X_{2S}), which takes into account only the mass loss related to the physical activation, X_{1S} accounts for the mass loss during the whole one-step process from the biomass feedstock. Hence, the burn-offs corresponding to the one-step activation process are, in all cases, numerically higher than those related to the two-step activation. In order to compare both production pathways in terms of yield of AC, the overall mass yield (y_{2S}) for the *2S* ACs was also calculated according to Eq. (3), where y_{char} is the mass yield of biochar (in mass fraction) after the pyrolysis step. The mass yield for *1S* ACs (y_{1S}) was calculated using Eq. (4).

$$y_{2S} = y_{char} \cdot (100 - X_{2S}) \tag{3}$$

$$y_{1S} = (100 - X_{1S}) \tag{4}$$

The textural characterization of the carbon materials was performed by N_2 and H_2 adsorption at -196 °C using an ASAP 2020 automatic adsorption device from Micromeritics (USA). Samples were outgassed under secondary vacuum at 110 °C for at least 48 h and outgassing at the same temperature for at least 6 h was also carried out in the analysis port. Warm and cold volumes were determined after analysis to avoid He entrapment in ultra-micropores. Processing of the adsorption isotherm data was performed using Microactive® and SAIEUS® software provided by Micromeritics. Pore size distributions (PSDs) and surface areas ($S_{2D-NLDFT}$) were calculated by applying the two-dimensional non-local density functional theory model for heterogenous surfaces (2D-NLDFT-HS) [36] to N_2 and H_2 isotherms simultaneously. The total pore volume (V_{tot}), ultra-micropore volume (V_{ultra}, < 0.7 nm), micropore volume (V_{micro}, <2 nm) and mesopore volume (V_{meso}, 2−50 nm) were obtained by integrating the PSDs in the corresponding pore size ranges.

Infrared spectra were performed in the wavenumbers range of 600—4000 cm^{-1} using a Fourier-Transform Infrared (FTIR) spectrometer (Frontier Spotlight 400, PerkinElmer, Japan).

2.5. Statistical analysis

An unreplicated 2-level full factorial design was adopted to evaluate the effects of the assessed pyrolysis process parameters. Three replicates at the center point were carried out to estimate the experimental error and the overall curvature effect [37]. The structure of the regression model (using normalized values for factors in the range from −1 to 1) used during statistical analysis for the response variables (i.e., textural properties of 2S ACs) was as follows:

$$\begin{aligned}
\widehat{y} = &\ \beta_0 + \beta_1 T + \beta_2 P + \beta_3 \tau + \beta_4 CO_2 + \beta_{12} T{\cdot}P + \beta_{13} T{\cdot}\tau \\
&+ \beta_{14} T{\cdot}CO_2 + \beta_{23} P{\cdot}\tau + \beta_{24} P{\cdot}CO_2 + \beta_{34}\tau{\cdot}CO_2 \\
&+ \beta_{123} T{\cdot}P{\cdot}\tau + \beta_{124} T{\cdot}P{\cdot}CO_2 + \beta_{134} T{\cdot}\tau{\cdot}CO_2 \\
&+ \beta_{234} P{\cdot}\tau{\cdot}CO_2
\end{aligned}$$

(5)

where β_0, β_i, β_{ij}, and β_{ijk} are the intercept, linear, 2-way interaction and 3-way interaction coefficients, respectively. The regression models used for the response variables related to the textural properties of the 1S ACs were the same as those described in Eq. (5) without considering the gas residence time as a factor. Statistical calculations were conducted using Minitab software (v17).

2.6. Adsorption isotherms and breakthrough simulations

CO_2 and CH_4 adsorption isotherms were measured up to 3.5 MPa, at 25 and 50 °C, using a HPVA II high-pressure manometric device (from Micromeritics). The samples were firstly outgassed under secondary vacuum (5×10^{-7} Pa) at 110 °C for at least 48 h. Afterwards, the pressure was gradually increased from 0.005 to 3.5 MPa, and then decreased stepwise to 0.5 MPa. The amount of gas adsorbed was calculated as the difference between the amount of gas dosed and the amount of gas determined at each equilibrium pressure.

The transient pressure change prior to the first isotherm point was recorded to obtain the adsorption kinetics. The batch kinetic model presented in Appendix A was fitted to the experimental kinetic data to obtain an estimate of the diffusivity of methane and carbon dioxide on the solid adsorbents.

The experimental data obtained from the isotherms were described using the Sips model. The ideal adsorbed solution theory (IAST) was adopted to predict the adsorption behavior of CO_2/CH_4 binary mixtures at different volume concentrations (i.e., 10:90 v/v, 30:70 v/v, 50:50 v/v, and 70:30 v/v). The selectivity towards CO_2 over CH_4, S, was then calculated as follows:

$$S = (x_{CO_2}\, y_{CH_4})\,/(x_{CH_4}\, y_{CO_2})$$

(6)

where x and y are the gas molar fractions in the adsorbed and gas phases, respectively.

Simulations of adsorption breakthrough curves were carried out at 0.1, 0.3, 0.5, 0.7 and 1.0 MPa considering an initial temperature of 30 °C and a total feed flow rate of 0.75 NL min^{-1}, with a molar composition of 40% CO_2 and 60% CH_4. A simulated fixed-bed column with length and diameter of 60 cm and 2.8 cm, respectively, was considered to run the simulations using gPROMS ModelBuilder.

The samples tapped densities were obtained in an Autotap

equipment of Quantachrome®. The bed porosity was calculated using the bed and particle densities as follows:

$$\varepsilon_{bed} = 1 - \rho_{bed}/\rho_{par}$$

(7)

where ρ_{bed} and ρ_{par} are the bed and particle densities, respectively. The particle density and porosity were measured by mercury porosimetry (Autopore IV, Micromeritics). The average particle diameter was measured by laser diffraction using a Mastersizer Hydro 3000 analyzer (Malvern instruments Ltd.) equipped with a Hydro LV sampler and a measurement cell for liquid phase suspensions.

More details regarding the IAST-based approach and the carbon adsorbents parameters used to run the simulations under dynamic conditions are given in Appendix A.

3. Results and discussion

The complete characterization of the WS pellets (including lignocellulosic composition, proximate, ultimate, and XRF analyses) is reported in Table A.1 (Appendix A). Furthermore, Appendix A also provides details on the pyrolysis behavior of WS pellets under either a pure N_2 atmosphere or a mixture of CO_2/N_2, including an assessment of repeatability and an analysis of mass loss profiles for the one-step activation experiments (see Figs. A.2 and A.3, respectively).

3.1. Conversion and textural properties of activated carbons

This section covers the results obtained from the full characterization of all ACs studied here. The numerical results are reported in Tables 1 and 2; more details on the statistics related to this section are given in Tables A.2 and A.3.

3.1.1. Two-step activation

When producing WS-derived ACs by slow pyrolysis and subsequent physical activation with CO_2 at 800 °C (two steps), the maximum pyrolysis temperature had a negative effect on the degree of burn-off (as shown in Fig. 2a). This could be explained by the fact that higher pyrolysis temperatures could lead to slightly more ordered carbon structures, making them less prone to reaction [38,39]. Similar conclusions can be drawn for the textural properties of the resulting ACs (see Fig. 2c—e), except for $V_{ultra\ (2S)}$, which appears to be positively affected by the maximum temperature and, to a greater extent, by the gas residence time. The effect of gas residence time also contributed to reduce the resulting X_{2S}, due to the importance of secondary charring reactions, which led to the formation of a more stable biochar structure. On the other hand, the effect of absolute pressure was found to be negative on both final specific surface area and porosity development (see Fig. 2b—e). This aspect could also be explained as a consequence of the formation of a more stable biochar during slow pyrolysis [40] and the clogging of its pores that would prevent the development of porosity during the activation step. It is important to note that it was not possible to develop mesoporosity under these activating conditions and, for this reason, $V_{meso\ (2S)}$ is not reported in Fig. 2. The presence of CO_2 as gas carrier in the pyrolysis environment did not affect the characteristics of the ACs, as well as the properties of the biochars produced, as previously reported [32]. This also indicates the possibility of recycling a flue gas stream by using it as a low-cost pyrolysis atmosphere, resulting in significant cost savings over N_2 on an industrial scale.

The values of surface areas and pore volumes obtained in this set of experiments were fully comparable to those obtained in a previous study [41] for WS-derived ACs produced by slow pyrolysis

Table 1
Experimental results of surface area ($S_{2D-NLDFT}$), ultramicropore volume (V_{ultra}), micropore volume (V_{micro}), mesopore volume (V_{meso}), total pore volume (V_{tot}) and burn-off (X) obtained in the two-step (2S) activation experiments.

Pyrolysis conditions				Response variable						
T (°C)	P (MPa)	τ (s)	CO_2 (vol. %)	$S_{2D-NLDFT\ (2S)}$ (m^2 g^{-1})	$V_{ultra\ (2S)}$ (cm^3 g^{-1})	$V_{micro\ (2S)}$ (cm^3 g^{-1})	$V_{meso\ (2S)}$ (cm^3 g^{-1})	$V_{tot\ (2S)}$ (cm^3 g^{-1})	X_{2S} (%)	y_{2S} (%)
400	0.9	200	60	905	0.16	0.25	0.02	0.27	45.3	17.3
400	0.9	100	60	837	0.11	0.24	0.02	0.26	51.3	15.1
550	0.2	100	0	906	0.17	0.25	0.03	0.28	42.6	15.8
400	0.2	100	60	986	0.11	0.30	0.05	0.35	63.7	10.6
550	0.9	200	0	905	0.15	0.25	0.02	0.27	37.1	17.9
550	0.2	100	60	865	0.15	0.24	0.02	0.26	45.4	15.3
475	0.55	150	30	933	0.15	0.26	0.03	0.29	44.5	16.3
400	0.9	100	0	782	0.09	0.25	0.02	0.27	56.0	14.6
400	0.9	200	0	955	0.17	0.27	0.03	0.29	49.4	16.4
400	0.2	100	0	919	0.15	0.25	0.02	0.27	49.4	15.7
550	0.9	100	0	870	0.15	0.24	0.03	0.27	48.8	14.1
550	0.2	200	0	945	0.17	0.26	0.02	0.28	38.5	17.5
550	0.9	100	60	899	0.15	0.25	0.03	0.28	49.0	14.2
475	0.55	150	30	915	0.17	0.25	0.04	0.28	48.5	15.0
550	0.9	200	60	860	0.16	0.24	0.04	0.27	42.9	16.0
475	0.55	150	30	940	0.17	0.26	0.03	0.28	45.0	16.3
550	0.2	200	60	916	0.16	0.25	0.02	0.27	36.2	18.4
400	0.2	200	60	998	0.17	0.28	0.02	0.30	47.9	17.3
400	0.2	200	0	957	0.18	0.26	0.02	0.28	47.1	17.3

Table 2
Same as Table 1, but for the one-step (1S) activation experiments.

Pyrolysis conditions			Response variable						
T (°C)	P (MPa)	CO_2 (vol. %)	$S_{2D-NLDFT\ (1S)}$ (m^2 g^{-1})	$V_{ultra\ (1S)}$ (cm^3 g^{-1})	$V_{micro\ (1S)}$ (cm^3 g^{-1})	$V_{meso\ (1S)}$ (cm^3 g^{-1})	$V_{tot\ (1S)}$ (cm^3 g^{-1})	X_{1S} (%)	y_{1S} (%)
700	0.55	37.5	661	0.14	0.14	—	0.14	70.1	29.9
750	0.9	75	882	0.14	0.26	0.02	0.28	78.5	21.5
750	0.2	0	523	0.12	0.12	—	0.12	68.3	31.7
750	0.2	75	760	0.14	0.19	0.01	0.20	71.3	28.7
700	0.55	37.5	669	0.14	0.15	—	0.15	70.0	30.0
650	0.9	0	537	0.12	0.12	—	0.12	68.2	31.8
700	0.55	37.5	700	0.14	0.15	0.02	0.17	69.9	30.1
650	0.9	75	606	0.13	0.13	—	0.13	69.2	30.8
750	0.9	0	400	0.10	0.10	—	0.10	69.2	30.8
650	0.2	0	574	0.12	0.12	—	0.12	67.9	32.1
650	0.2	75	625	0.13	0.13	—	0.13	67.8	32.2

(500 °C, atmospheric pressure, and 5 °C min^{-1} as heating rate) and subsequent activation at 700—850 °C and 0.1—1.0 MPa under a pure CO_2 atmosphere. In particular, ACs obtained from biochars produced at 400 °C and 0.2 MPa showed, in some cases, better textural properties than those produced under similar conditions in the above-mentioned work (even when high pressures were applied to promote the extent of the reverse Boudouard reaction during the activation step). This finding seems to demonstrate the pivotal role that the pyrolysis operating conditions play in determining the textural properties of the resulting ACs. Table 1 shows that the AC with the highest surface area (998 cm^2 g^{-1}) and the most developed porosity was obtained from a biochar produced at 400 °C and 0.2 MPa, confirming the considerations explained in this section.

3.1.2. One-step activation

Fig. 3a shows the influence of the process operating conditions on the burn-off (X_{1S}) during the one-step production of ACs. As expected, the main factor affecting mass loss was the maximum temperature; its increase from 650 to 750 °C led to a higher carbonization degree, due to a more pronounced thermal degradation of the biomass constituents [42,43]. Even though the effect was smaller, the presence of CO_2 as an activating agent also contributed to increase the burn-off, as a clear consequence of the gasification of the carbonaceous matrix. Overall, the lowest value of X_{1S} was 67.8%, corresponding to the mildest temperature (650 °C),

whereas the highest value (78.5%) was obtained at 750 °C under an atmosphere containing CO_2. It is important to remember that the X_{1S} values took into account the mass loss related to the pyrolysis step too; for this reason, they resulted to be higher than the X_{2S} values.

According to a previous study conducted on the pyrolysis of WS pellets [32], it was confirmed that absolute pressure does not have a significant effect on the final yield of the resulting carbon material. The role of CO_2 atmosphere and, to a lesser extent, maximum temperature, was predominant for the development of porosity; indeed, their significant effects on the surface area and pores volumes are clearly visible in Fig. 3b—e. In contrast to the previous work [32], which was performed at lower maximum pyrolysis temperatures (400—550 °C), the ultra-micropore volume did not appear to be affected by the maximum temperature, which generally leads to greater thermal degradation of biomass, followed by additional evolution of volatiles, resulting in the creation of new pores. This discrepancy is probably due to the higher maximum temperatures used in this work; in particular, the higher the temperature, the lower its effect on $V_{ultra\ (1S)}$. Similar to what was observed for the two-step activation process, $V_{meso\ (1S)}$ was not reported in Fig. 3 due to the lack of mesopore formation. Even though the reactor configuration was designed for maximizing the biochar yield (i.e., enhancing secondary charring reactions through a slow release of primary volatiles at the inter-particle level) rather
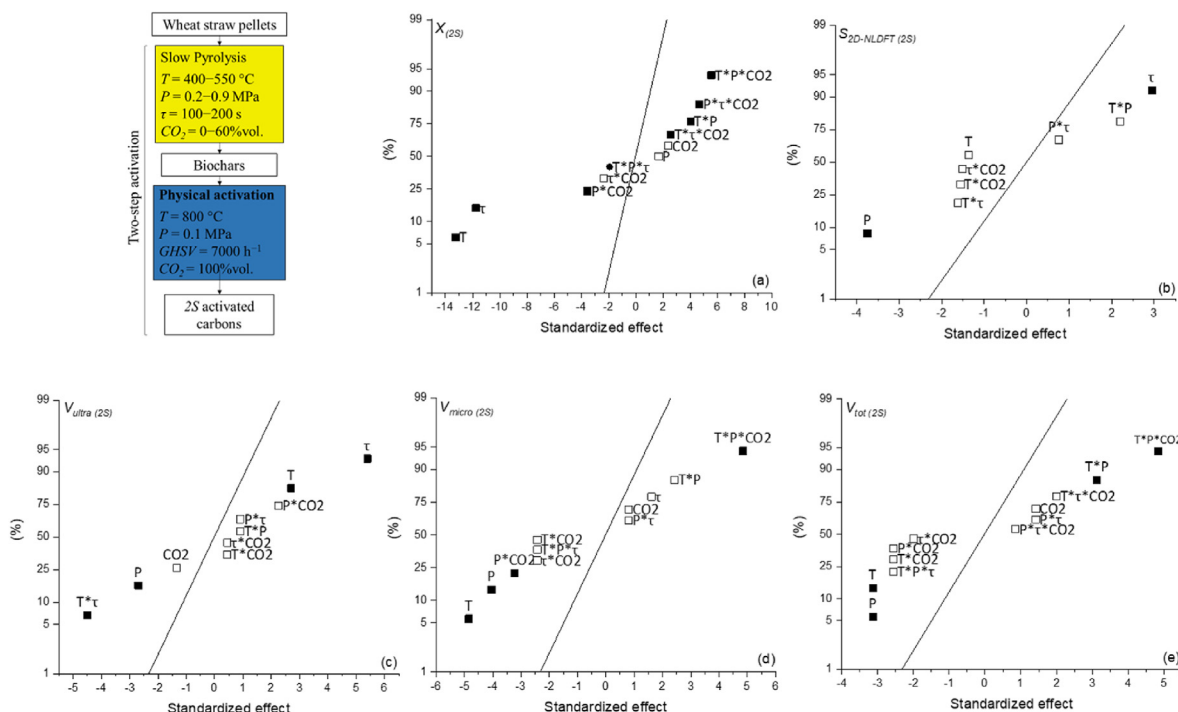
Fig. 2. Normal plot of the standardized effects ($\alpha = 0.05$) for ACs produced by two-step (*2S*) activation: (a) burn-off (X); (b) surface area ($S_{2D-NLDFT}$); (c) ultramicropore volume (V_{ultra}); (d) micropore volume (V_{micro}); and (e) total pore volume (V_{tot}) (squares = significant effect; empty squares = non-significant effect; the straight line represents the null-effect points).
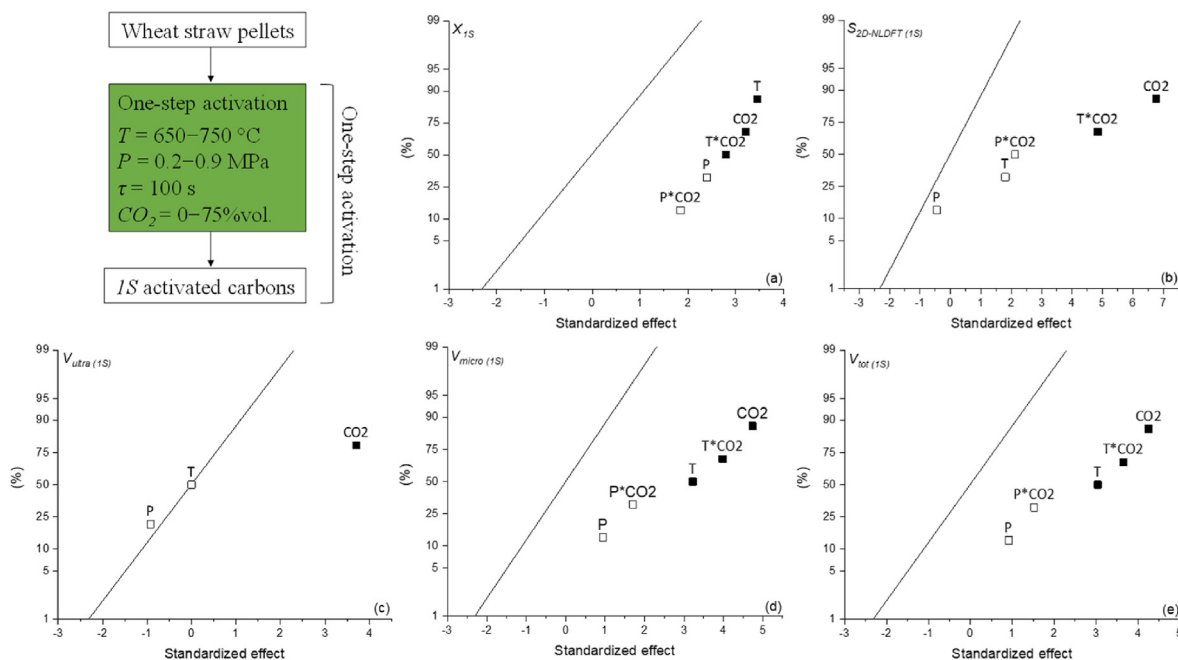

Fig. 3. Same as Fig. 2, but ACs produced by one-step (*1S*) activation: (a) burn-off (X), (b) ultramicropore volume (V_{ultra}), (c) micropore volume (V_{micro}), (d) mesopore volume (V_{meso}) and (e) total pore volume (V_{tot}) (square, significant effect; empty square, non-significant effect; the straight line represents the null-effect points).

than for activating the biochar, and keeping in mind the relatively milder temperatures employed, the surface areas as well as the porosity development of the *1S* ACs were only slightly lower than those obtained for *2S* ACs. In fact, the best one-step AC (produced at 750 °C and 0.9 MPa) showed textural properties very similar to those reported for the two-step ACs. Moreover, the *1S* ACs showed a higher final mass yield in comparison to that related to the *2S* ACs, which resulted to be almost twice higher in all cases (see Tables 1 and 2, respectively). The reason behind this discrepancy between the two production routes is mainly due to the different activation conditions adopted, especially in terms of maximum temperature and CO_2 concentration in the reactor atmosphere, which were more

severe during the *2S* activation process. These outstanding results demonstrate that one-step pressurized activation might be a valuable alternative to the conventional two-step activation, due to its lower energy cost and higher efficiency in terms of processing time and production capacity.

3.2. FT-IR spectra and surface chemistry

The results of FT-IR spectroscopy measurements for *2S* ACs are shown in Fig. A.4a. The samples were mainly characterized by methylene groups (1460 cm^{-1}), aromatic rings (1450–1600 cm^{-1}) and, in some cases, OH groups (3500 cm^{-1}). The bands showed relatively small differences in intensity, meaning that the number of retained functional groups in the *2S* ACs was not significantly influenced by the pyrolysis operating conditions. Conversely, more intense bands, for the aforementioned functional groups, were visible for *1S* ACs (see Fig. A.4b), even at the highest maximum temperature (750 °C). This finding may be ascribed to differences in the reactor configuration as well as in the different temperature conditions and CO_2 concentrations employed during the synthesis of *2S* and *1S* ACs.

3.3. CO_2 adsorption capacity and selectivity CO_2/CH_4

The ACs with the highest surface area and porosity (three *2S* carbons and three *1S* carbons) were selected for CO_2 and CH_4 adsorption experiments. The tested carbon materials are reported in Table 3. The Sips isotherm model (see Appendix A for further details) was fitted simultaneously to the experimental data at different temperature for each material. The parameters obtained by fitting the isotherm model are presented in Table A.4, and were used to perform the IAST-based and breakthrough simulations. The experimental isotherm data were also used to calculate the average heat of adsorption by means of the Clausius-Clapeyron equation. The average heat of adsorption is presented in Table A.8, and was then used to simulate the non-isothermal adsorption breakthrough curves.

According to the observations reported in Section 3.1.1, the combination of lower temperatures and pressures and higher gas residence time during the pyrolysis step proved to be crucial for obtaining *2S* carbons with high surface areas and developed porosity. As expected, the molar amounts of CO_2 and CH_4 adsorbed at equilibrium conditions increased with pressure and decreased with temperature (see Fig. 4). Furthermore, the slope of the isotherm became less steep with increasing pressure because the adsorption sites are closer to saturation under these conditions. Fig. 4 also shows that the CO_2 and CH_4 adsorption isotherms were fully reversible, indicating physical adsorption [4]. All WS-derived ACs preferentially adsorbed CO_2 over CH_4, due to the higher quadrupole moment of CO_2 [14,44], which promotes a stronger attraction between the adsorbate and the adsorbent surface.

Overall, *2S* ACs reached higher CO_2 uptake capacity than *1S* ACs

when the pressure was increased to 3.5 MPa. However, the performances of *2S* and *1S* ACs were perfectly comparable at lower pressures (0–0.5 MPa). The CO_2 uptake capacity at 0.1 MPa of the ACs produced in this study is compared with those of carbon-based adsorbents reported from previous studies in Table A.5. It is easy to observe that our ACs exhibited somewhat higher adsorbed amounts of CO_2 than many in the literature, regardless of their higher surface areas (up to 3000 m^2 g^{-1}) and even though they were tested at lower temperatures (i.e., 20 °C) in some cases.

Fig. 5a shows the CO_2/CH_4 selectivity values under 10 vol % CO_2, which were calculated using the IAST method after fitting the Sips equation to the isotherms. The selectivity profiles of the ACs were not visibly affected by the variation of the CO_2/CH_4 concentration ratio; for this reason, the selectivity profiles at higher CO_2 content are reported in Appendix A (see Fig. A.5). At pressures below 0.5 MPa, all samples showed high values of selectivity (up to more than 10) and these decreased with increasing pressure. Some authors have claimed that the predominant effect of the CO_2-sorbent interaction due to the basic functionalities on the surface [45]. However, it has been shown that it is only true for working pressures below 0.5 MPa. The shift from surface chemistry-controlled to pore texture-controlled behavior occurs at 0.5 MPa [46]. The latter study is in good agreement with the present results. By increasing the pressure above 1.0 MPa, the *2S* ACs showed a slight tendency to increase in selectivity, which was accentuated when the CO_2 concentration was higher. According to Castrillon et al. [4], the proportional increase in selectivity with pressure could probably be due to the intrinsic shape of the CO_2 and CH_4 isotherms; in other words, CO_2 uptake was positively affected by pressure to a greater extent than CH_4 uptake. On the other hand, the small increase in selectivity at higher CO_2 concentrations seems to be in disagreement with the reported literature [4]. This result is probably due to a combination of factors, such as PSD, micropore volume and surface area of the samples. The effect of CO_2 concentrations on selectivity at high pressures was even more visible for the *1S* AC produced at 700 °C, 0.55 MPa, 100 s and 37.5 vol % CO_2, whereas the selectivity related to the other *1S* ACs remained approximately constant after the initial decrease. Overall, the *2S-3* sample appeared to be the best AC in terms of CO_2 retention, showing higher selectivity regardless of pressure and CO_2 content (see Fig. 5b for the corresponding set of selectivity profiles).

In conclusion, the resulting selectivity values were notably high for all ACs produced in this study, in most cases even higher than those reported in previous studies (see Table A.6) and examined under the same conditions. In addition, the CO_2/CH_4 selectivity profiles under 10, 30, 50 and 70 vol % CO_2 of a commercial AC (from *Brascarbo Agroindustrial Ldta.*, Brazil) [47] were also calculated using the IAST method (see Fig. A.6) for further comparison purposes. In line with the above-reported findings, the AC from *Brascarbo* showed slightly lower selectivity values, despite being examined under the same conditions and having a surface area totally comparable with those of *1S* and *2S* ACs.

Table 3
Activated carbons selected for CO_2 and CH_4 adsorption experiments.

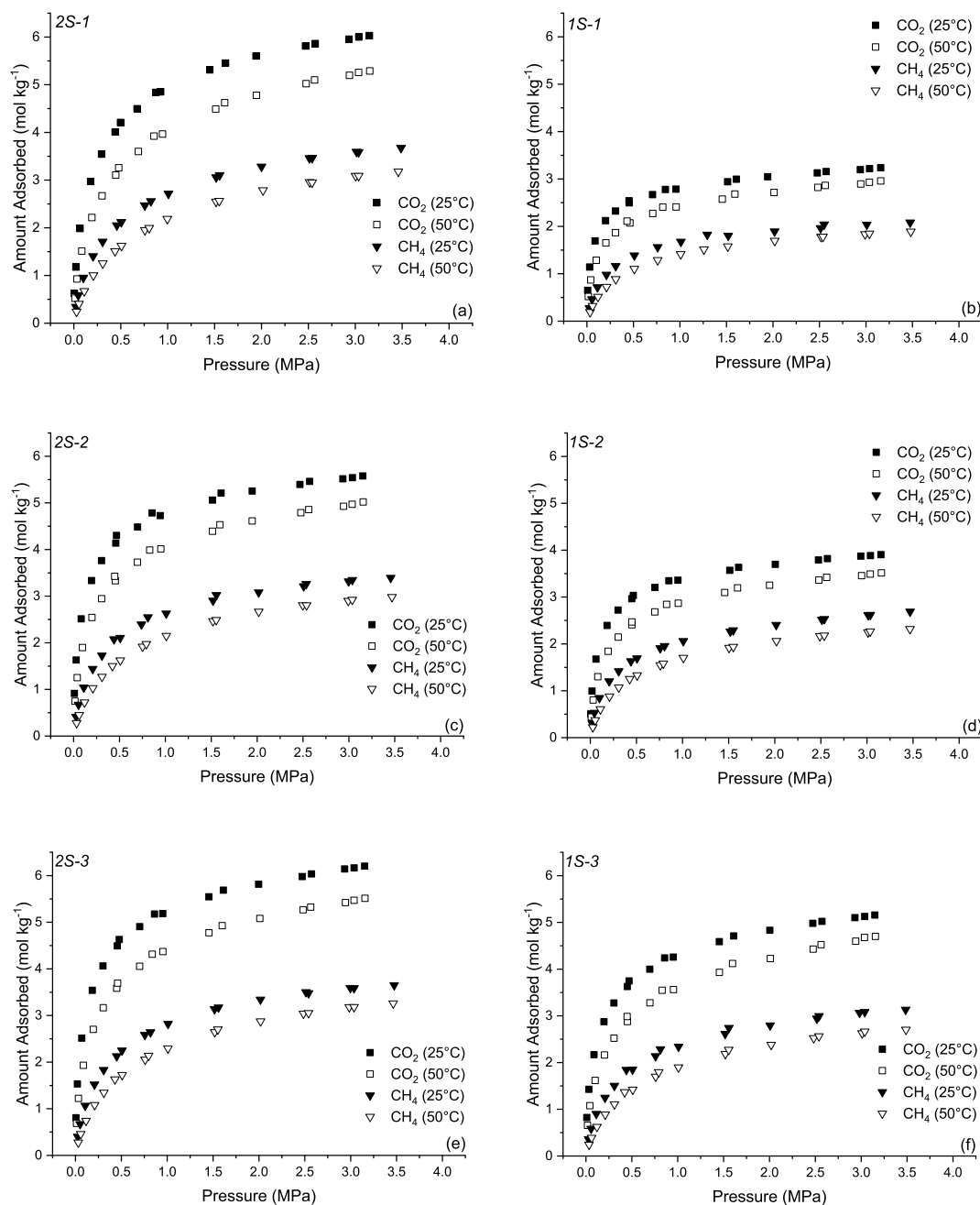| Type of activation	AC	Slow Pyrolysis				CO_2 activation			
		T (°C)	P (MPa)	τ (s)	CO_2 (vol. %)	T (°C)	P (MPa)	τ (s)	CO_2 (vol. %)
One-Step	*1S-1*	–	–	–	–	700	0.55	100	37.5
	1S-2	–	–	–	–	750	0.2	100	75
	1S-3	–	–	–	–	750	0.9	100	75
Two-Step	*2S-1*	400	0.2	100	60	800	0.1	–	100
	2S-2	400	0.2	200	0	800	0.1	–	100
	2S-3	400	0.2	200	60	800	0.1	–	100

Fig. 4. CO_2 and CH_4 adsorption isotherms for selected 1S and 2S activated carbons (see Table 3 for details on production process conditions).

3.4. Simulated breakthrough curves

Although the IAST model is a suitable method to predict the separation selectivity of ACs, the study of their performance under dynamic conditions remains an essential step before any application. Fig. 6a–b show, respectively, the simulated CH_4 and CO_2 breakthrough curves at 0.5 MPa for each AC, whereas the fixed bed parameters used for the simulations are reported in Table 4. Additional parameters used in the simulation of the adsorption breakthrough, such as those related to the adsorption isotherms, kinetics, and thermodynamics, are given in Appendix A (Tables A.4, A.7 and A.8, respectively). The full set of breakthrough simulations for the selected ACs are available in Figs. A.7−A.12. In all simulations, methane breakthrough occurred before carbon dioxide

breakthrough, indicating the ability of all materials to achieve methane separation from mixtures with carbon dioxide. This is due to the fact that CH_4 is a completely non-polar molecule and interacts very weakly with most materials. While CO_2 has a quadrupolar moment and so it interacts, both physically and chemically, with the ACs surface. In addition, the adsorption breakthrough curves shown in Figs. A.7−A.12 indicated that the retention time of both gases increased with operating pressure.

As expected, Fig. 6a shows that the CH_4 stoichiometry time (i.e., the time needed to reach 50% of the feed flow rate at the reactor outlet, represented by $t^*_{CH_4}$) at 0.5 MPa was shorter, between 9 and 14 min, than that of CO_2, $t^*_{CO_2}$, which ranged from 34 to 43 min (Fig. 6b). In addition, in Fig. 6a, it is possible to observe the typical
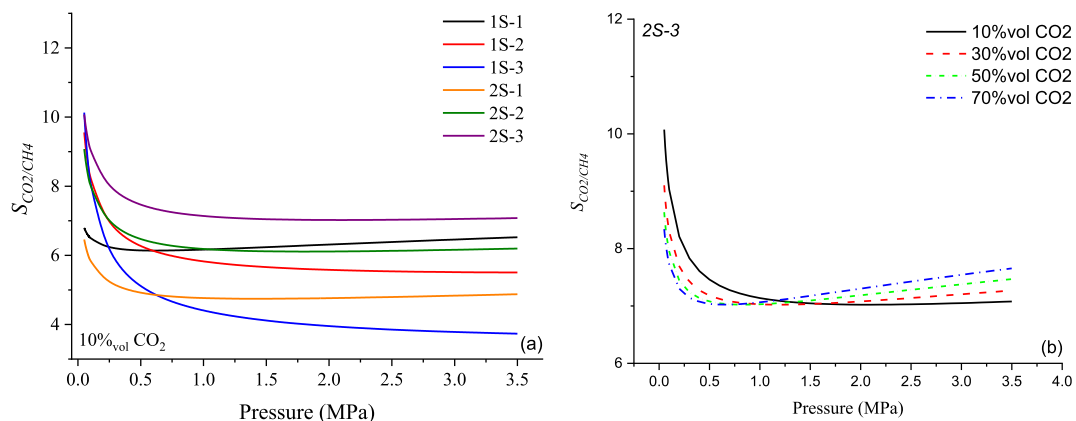
Fig. 5. (a) IAST-based selectivity values for ACs tested under 10 vol % CO_2; and (b) selectivity profiles of 2S−3 AC under 10, 30, 50, and 70 vol % CO_2.
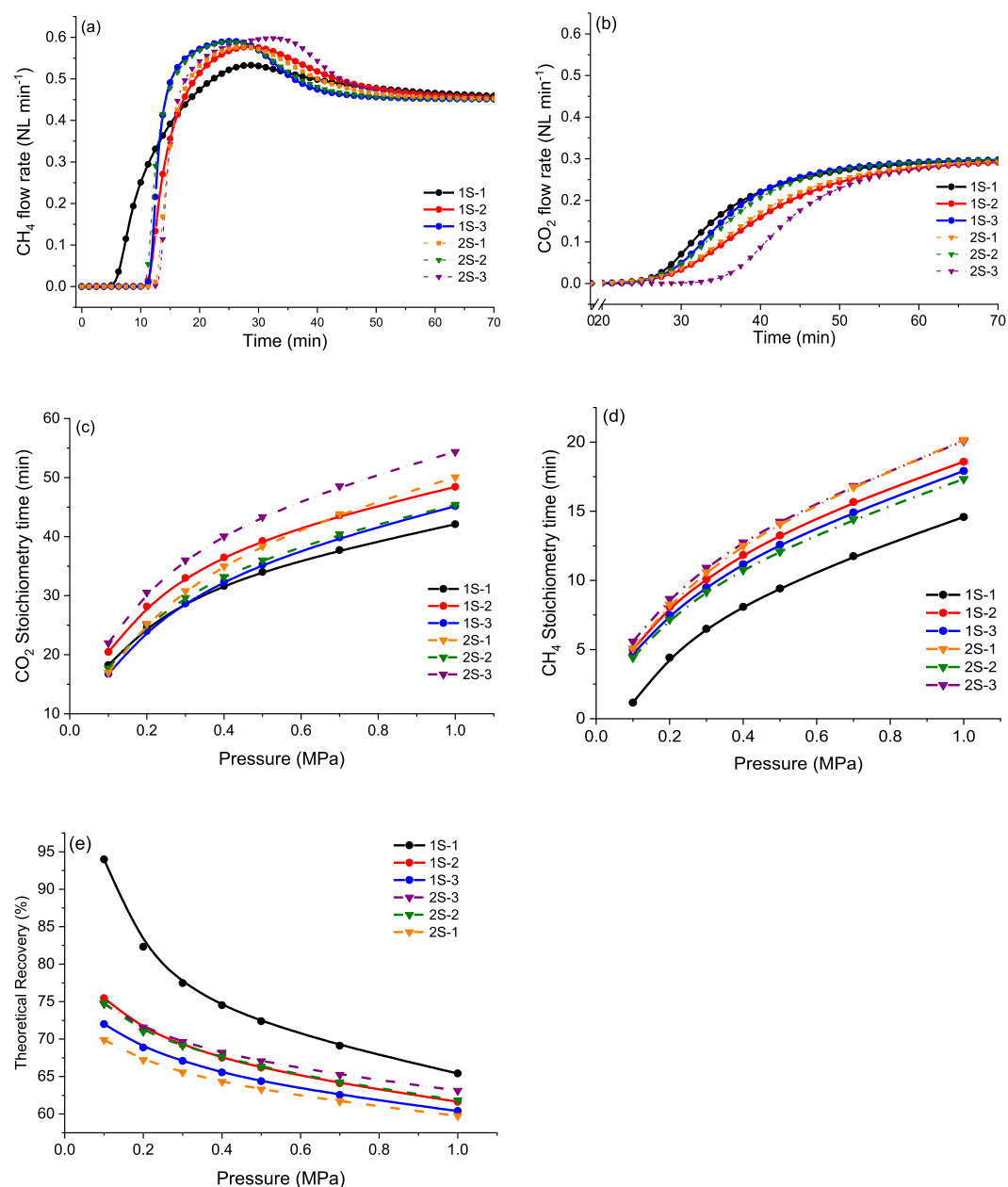

Fig. 6. Simulated results for (a) CH_4 and (b) CO_2 breakthrough curves at 0.5 MPa and 30 °C; (c) CH_4 and (d) CO_2 adsorption stoichiometry times as function of adsorption pressure; and (e) theoretical CH_4 recovery as a function of adsorption pressure.

Table 4
Fixed bed parameters used for the breakthrough simulations.

Activated carbon	Bed density (kg m^{-3})	Bed porosity (—)	Particle density (kg m^{-3})	Particle porosity (—)	Average particle diameter (mm)
1S-1	599	0.534	1285	0.431	0.14
1S-2	603	0.493	1190	0.474	0.30
1S-3	450	0.716	1586	0.298	0.22
2S-1	471	0.602	1184	0.476	0.32
2S-2	391	0.660	1149	0.491	0.41
2S-3	433	0.626	1158	0.488	0.34

roll-over phenomena, consisting of a temporary excess of CH_4 flow rate over the feed concentration, due to the replacement of CH_4 by CO_2 on the sorbent surface [5]. During an adsorption separation process, $t^*_{CO_2}$ and $t^*_{CH_4}$ represent the limits of the operation time; from an industrial point of view, longer CO_2 stoichiometry times are strongly desired in order to ensure longer operation times. Conversely, shorter values of $t^*_{CH_4}$ are required, as they are directly related to the amount of CH_4 desorbed from the solid phase. Given that both $t^*_{CO_2}$ and $t^*_{CH_4}$ are direct functions of the respective gas amounts adsorbed at equilibrium, they strictly depend on the breakthrough pressure, as shown in Fig. 6c—d. These figures also confirmed that CH_4 broke through earlier than CO_2, regardless of the pressure considered. Overall, the *2S* AC obtained from the biochar produced at 400 °C, 0.2 MPa, 200 s under a 60 vol % CO_2 atmosphere (*2S-3*) showed the highest t^* values over the whole range of pressures adopted during all experiments, in line with its high selectivity observed in the previous section.

Since the pure CH_4 flow rate definitely leaves the adsorption column in the time interval between $t^*_{CO_2}$ and $t^*_{CH_4}$, the amount of pure CH_4 released during the adsorption process directly depends on both stoichiometric times. Taking this aspect into account, it is possible to calculate a theoretical CH_4 recovery from the adsorption process as:

$$Recovery_{CH_4} = (t^*_{CO_2} - t^*_{CH_4}) \big/ t^*_{CO_2} \qquad (6)$$

The theorical CH_4 recovery values obtained for the examined ACs (see Fig. 6e) highlighted the *1S* AC produced at 700 °C, 0.55 MPa, 100 s under a 37.5 vol % CO_2 atmosphere (*1S-1*) as the sorbent with the highest theoretical recovery, reaching around 95% at 0.1 MPa, and dropping to about 70% at 1.0 MPa. This result, clearly in contrast to the findings obtained by IAST methodology, is mainly due to the effects of various factors disregarded in the aforementioned IAST model, such as slow CH_4 diffusion and different packing densities (see Table 4). Furthermore, breakthrough simulations also predicted temperature increases around 25 °C inside the fixed-bed column (see Figs. A.6—A.11), which could also have a considerable effect on the adsorption process performance. Another parameter not considered in the IAST model, which certainly affected CH_4 recovery, was the average particle diameter, in particular, the smaller the particles, the higher the recovery. The CH_4 recovery values obtained for the *1S* and *2S* ACs were similar to many adsorbents reported in the literature (see Table A.9), although it is important to keep in mind that the operating pressures were milder than those employed in this work.

4. Conclusions

Sustainable activated carbons (ACs) from wheat straw (WS) biomass were produced by one-step (*1S*) and two-step (*2S*) physical activation processes. The obtained outcomes indicate that, for wheat straw and the range of operating conditions adopted, the one-step ACs exhibit similar textural features as ACs synthetized via a traditional two-step pathway. Interestingly, the *1S* ACs can be produced at considerably higher mass yields, which makes them attractive for commercial exploitation. Furthermore, *1S* and *2S* ACs exhibited even higher CO_2 uptakes and CO_2/CH_4 selectivity values than several adsorbents reported in the literature, proving that they are absolutely feasible for CH_4/CO_2 separation. In particular, the *2S* AC produced at 400 °C, 0.2 MPa, 200 s and 60 vol % CO_2 showed the highest IAST-based selectivity, regardless of the CO_2 concentration and pressure conditions applied. However, breakthrough simulations revealed that the *1S* AC produced at 700 °C, 0.55 MPa, 100 s and 37.5 vol % CO_2 showed the best CH_4 recovery performance under dynamic conditions. These notable findings highlighted *1S* physical activation at moderate pressure as a promising route to produce carbon-based adsorbents, which may replace the conventional *2S* physical activation process and lead to remarkable improvements, especially on an industrial scale. Indeed, *1S* physical activation would allow a significant reduction in operating and installation costs as well as an improvement in productivity.

CRediT authorship contribution statement

Gianluca Greco: Conceptualization, Methodology, Software, Validation, Formal analysis, Investigation, Data curation, Writing — original draft, Resources. **Rafael L.S. Canevesi:** Conceptualization, Data curation, Methodology, Investigation, Resources, Software, Formal analysis, Writing — original draft. **Christian Di Stasi:** Data curation, Methodology, Investigation, Resources. **Alain Celzard:** Data curation, Resources, Supervision, Writing — review & editing. **Vanessa Fierro:** Data curation, Methodology, Resources, Supervision, Writing — review & editing. **Joan J. Manyà:** Resources, Writing — review & editing, Visualization, Supervision, Project administration.

Declaration of competing interest

The authors declare that they have no known competing financial interests or personal relationships that could have appeared to influence the work reported in this paper.

Acknowledgments

Appendix A. Supplementary data

Supplementary data to this article can be found online at https://doi.org/10.1016/j.renene.2022.04.035.

Nomenclature

$m_{biochar}$	mass of biochar
$m_{biomass}$	mass of biomass
m_f	final mass of the sample
$S_{2D-NLDFT}$	surface area
$S_{CO2/CH4}$	CO_2 selectivity over CH_4
V_{meso}	mesopore volume
V_{micro}	micropore volume
V_{tot}	total pore volume
V_{ultra}	ultra-micropore volume
X_i	burn-off
y_{char}	biochar yield
y_i	mass yield
ρ_{bed}	bed density
ρ_{par}	particle density

Acronyms

FT-IR	Fourier-Transform Infrared spectroscopy
GHSV	gas-hourly space velocity
IAST	Ideal Adsorbed Solution Theory
MEA	Mono-Ethanolamine
PSD	pore size distribution
1S	one-step activation
2S	two-step activation
XRF	X-Ray Fluorescence
WS	Wheat Straw

References

[1] N. Yang, R. Wang, Sustainable technologies for the reclamation of greenhouse gas CO_2, J. Clean. Prod. 103 (2015) 784—792, https://doi.org/10.1016/j.jclepro.2014.10.025.

[2] E.S. Shuba, D. Kifle, Microalgae to biofuels: 'Promising' alternative and renewable energy, review, Renew. Sustain. Energy Rev. 81 (2018) 743—755, https://doi.org/10.1016/j.rser.2017.08.042.

[3] G. Goula, V. Kiousis, L. Nalbandian, I. V Yentekakis, Catalytic and electrocatalytic behavior of Ni-based cermet anodes under internal dry reforming of CH_4+CO_2 mixtures in SOFCs, Solid State Ionics 177 (2006) 2119—2123, https://doi.org/10.1016/j.ssi.2006.03.040.

[4] M.C. Castrillon, K.O. Moura, C.A. Alves, M. Bastos-Neto, D.C.S. Azevedo, J. Hofmann, J. Möllmer, W.-D. Einicke, R. Gläser, CO_2 and H_2S removal from CH_4-rich streams by adsorption on activated carbons modified with K_2CO_3, NaOH, or Fe_2O_3, Energy Fuel. 30 (2016) 9596—9604, https://doi.org/10.1021/acs.energyfuels.6b01667.

[5] I. Durán, N. Álvarez-Gutiérrez, F. Rubiera, C. Pevida, Biogas purification by means of adsorption on pine sawdust-based activated carbon: impact of water vapor, Chem. Eng. J. 353 (2018) 197—207, https://doi.org/10.1016/j.cej.2018.07.100.

[6] B.P. Spigarelli, S.K. Kawatra, Opportunities and challenges in carbon dioxide capture, J. CO_2 Util. 1 (2013) 69—87, https://doi.org/10.1016/j.jcou.2013.03.002.

[7] X. Zhang, X. He, T. Gundersen, Post-combustion carbon capture with a gas separation membrane: parametric study, capture cost, and exergy analysis, Energy Fuel. 27 (2013) 4137—4149, https://doi.org/10.1021/ef3021798.

[8] J. Baxter, Z. Bian, G. Chen, D. Danielson, M.S. Dresselhaus, A.G. Fedorov, T.S. Fisher, C.W. Jones, E. Maginn, U. Kortshagen, A. Manthiram, A. Nozik, D.R. Rolison, T. Sands, L. Shi, D. Sholl, Y. Wu, Nanoscale design to enable the revolution in renewable energy, Energy Environ. Sci. 2 (2009) 559—588, https://doi.org/10.1039/B821698C.

[9] R. Ben-Mansour, M.A. Habib, O.E. Bamidele, M. Basha, N.A.A. Qasem, A. Peedikakkal, T. Laoui, M. Ali, Carbon capture by physical adsorption: materials, experimental investigations and numerical modeling and simulations — a review, Appl. Energy 161 (2016) 225—255, https://doi.org/10.1016/j.apenergy.2015.10.011.

[10] N.A. Rashidi, S. Yusup, An overview of activated carbons utilization for the post-combustion carbon dioxide capture, J. CO_2 Util. 13 (2016) 1—16, https://doi.org/10.1016/j.jcou.2015.11.002.

[11] C.A. Grande, Advances in pressure swing adsorption for gas separation, ISRN Chem. Eng. 2012 (2012), 982934, https://doi.org/10.5402/2012/982934.

[12] F. Dreisbach, R. Staudt, J.U. Keller, High pressure adsorption data of methane, nitrogen, carbon dioxide and their binary and ternary mixtures on activated carbon, Adsorption 5 (1999) 215—227, https://doi.org/10.1023/A:1008914703884.

[13] J. McEwen, J.-D. Hayman, A. Ozgur Yazaydin, A comparative study of CO_2, CH_4 and N_2 adsorption in ZIF-8, Zeolite-13X and BPL activated carbon, Chem. Phys. 412 (2013) 72—76, https://doi.org/10.1016/j.chemphys.2012.12.012.

[14] M. Álvarez-Gutiérrez, N. Victoria Gil, F. Rubiera, C. Pevida, Cherry-stones-based activated carbons as potential adsorbents for CO_2/CH_4 separation: effect of the activation parameters, Greenh. Gases Sci. Technol. 5 (2015) 812—825, https://doi.org/10.1002/ghg.1534.

[15] Y. Zheng, Q. Li, C. Yuan, Q. Tao, Y. Zhao, G. Zhang, J. Liu, Influence of temperature on adsorption selectivity: coal-based activated carbon for CH_4 enrichment from coal mine methane, Powder Technol. 347 (2019) 42—49, https://doi.org/10.1016/j.powtec.2019.02.042.

[16] D. Peredo-Mancilla, C.M. Ghimbeu, B.-N. Ho, M. Jeguirim, C. Hort, D. Bessieres, Comparative study of the CH_4/CO_2 adsorption selectivity of activated carbons for biogas upgrading, J. Environ. Chem. Eng. 7 (2019) 103368, https://doi.org/10.1016/j.jece.2019.103368.

[17] Y. Zhao, X. Liu, Y. Han, Microporous carbonaceous adsorbents for CO_2 separation via selective adsorption, RSC Adv. 5 (2015) 30310—30330, https://doi.org/10.1039/C5RA00569H.

[18] J. Park, N.F. Attia, M. Jung, M.E. Lee, K. Lee, J. Chung, H. Oh, Sustainable nanoporous carbon for CO_2, CH_4, N_2, H_2 adsorption and CO_2/CH_4 and CO_2/N_2 separation, Energy 158 (2018) 9—16, https://doi.org/10.1016/j.energy.2018.06.010.

[19] P. Kluson, S. Scaife, Microporous adsorbents for a selective separation of carbon dioxide from mixtures with methane and nitrogen, Chem. Biochem. Eng. Q. 16 (2002) 97—103, https://doi.org/10.15255/CABEQ.2014.635.

[20] R.B. Rios, H.R. Stragliotto, F.M. Peixoto, A.E.B. Torres, J. Bastos-Neto, M. Azevedo, D.C.S. Cavalcante, C, L, Studies on the adsorption behavior of CO_2-CH_4 Mixtures using activated carbon, Braz. J. Chem. Eng. 30 (2013) 939—951, https://doi.org/10.1590/S0104-66322013000400024.

[21] O. Mašek, P. Brownsort, A. Cross, S. Sohi, Influence of production conditions on the yield and environmental stability of biochar, Fuel 103 (2013) 151—155, https://doi.org/10.1016/j.fuel.2011.08.044.

[22] F. Ronsse, S. van Hecke, D. Dickinson, W. Prins, Production and characterization of slow pyrolysis biochar: influence of feedstock type and pyrolysis conditions, GCB Bioenergy 5 (2013) 104—115, https://doi.org/10.1111/gcbb.12018.

[23] J.J. Manyà, B. González, M. Azuara, G. Arner, Ultra-microporous adsorbents prepared from vine shoots-derived biochar with high CO_2 uptake and CO_2/N_2 selectivity, Chem. Eng. J. 345 (2018) 631—639, https://doi.org/10.1016/j.cej.2018.01.092.

[24] M. Molina-Sabio, M.T. Gonzalez, F. Rodriguez-Reinoso, A. Sepúlveda-Escribano, Effect of steam and carbon dioxide activation in the micropore size distribution of activated carbon, Carbon N. Y. 34 (1996) 505—509, https://doi.org/10.1016/0008-6223(96)00006-1.

[25] M.G. Plaza, A.S. González, J.J. Pis, F. Rubiera, C. Pevida, Production of microporous biochars by single-step oxidation: effect of activation conditions on CO_2 capture, Appl. Energy 114 (2014) 551—562, https://doi.org/10.1016/J.APENERGY.2013.09.058.

[26] A. Linares-Solano, J. De D. López-González, M. Molina-Sabio, F. Rodriguez-Reinoso, Active carbons from almond shells as adsorbents in gas and liquid phases, J. Chem. Technol. Biotechnol. 30 (1980) 65—72, https://doi.org/10.1002/jctb.503300109.

[27] A.C. Lua, J. Guo, Activated carbon prepared from oil palm stone by one-step CO_2 activation for gaseous pollutant removal, Carbon N. Y. 38 (2000) 1089—1097, https://doi.org/10.1016/S0008-6223(99)00231-6.

[28] K. Yang, J. Peng, H. Xia, L. Zhang, C. Srinivasakannan, S. Guo, Textural characteristics of activated carbon by single step CO_2 activation from coconut shells, J. Taiwan Inst. Chem. Eng. 41 (2010) 367—372, https://doi.org/10.1016/j.jtice.2009.09.004.

[29] A.S. González, M.G. Plaza, F. Rubiera, C. Pevida, Sustainable biomass-based carbon adsorbents for post-combustion CO_2 capture, Chem. Eng. J. 230 (2013) 456—465, https://doi.org/10.1016/j.cej.2013.06.118.

[30] D. Bergna, T. Varila, H. Romar, U. Lassi, Comparison of the properties of activated carbons produced in one-stage and two-stage processes, J. Carbon Res. 4 (2018), https://doi.org/10.3390/c4030041.

[31] G. Greco, M. Videgain, C. Di Stasi, B. González, J.J. Manyà, Evolution of the mass-loss rate during atmospheric and pressurized slow pyrolysis of wheat straw in a bench-scale reactor, J. Anal. Appl. Pyrolysis 136 (2018) 18—26, https://doi.org/10.1016/j.jaap.2018.11.007.

[32] G. Greco, C. Di Stasi, T. Rego, B. González, J.J. Manyà, Effects of slow-pyrolysis conditions on the products yields and properties and on exergy efficiency: a comprehensive assessment for wheat straw, Appl. Energy 279 (2020), https://doi.org/10.1016/j.apenergy.2020.115842.

[33] J.J. Manyà, M.A. Ortigosa, S. Laguarta, J.A. Manso, Experimental study on the effect of pyrolysis pressure, peak temperature, and particle size on the potential stability of vine shoots-derived biochar, Fuel 133 (2014) 163—172, https://doi.org/10.1016/j.fuel.2014.05.019.

[34] L. Wang, Ø. Skreiberg, M. Gronli, G.P. Specht, M.J. Antal, Is elevated pressure required to achieve a high fixed-carbon yield of charcoal from biomass? Part 2: the importance of particle size, Energy Fuels 27 (2013) 2146—2156, https://doi.org/10.1021/ef400041h.

[35] C. Di Stasi, D. Alvira, G. Greco, B. González, J.J.J.J. Manyà, Physically activated wheat straw-derived biochar for biomass pyrolysis vapors upgrading with high resistance against coke deactivation, Fuel 255 (2019), 115807, https://doi.org/10.1016/j.fuel.2019.115807.

[36] J. Jagiello, J. Kenvin, C.O. Ania, J.B. Parra, A. Celzard, V. Fierro, Exploiting the

adsorption of simple gases O2 and H2 with minimal quadrupole moments for the dual gas characterization of nanoporous carbons using 2D-NLDFT models, Carbon N. Y. 160 (2020) 164–175, https://doi.org/10.1016/j.carbon.2020.01.013.

[37] D.C. Montgomery, Design and Analysis of Experiments, sixth ed., 2005. Hoboken.

[38] F. Min, M. Zhang, Y. Zhang, Y. Cao, W.-P. Pan, An experimental investigation into the gasification reactivity and structure of agricultural waste chars, J. Anal. Appl. Pyrolysis 92 (2011) 250–257, https://doi.org/10.1016/J.JAAP.2011.06.005.

[39] W. Zhu, W. Song, W. Lin, Catalytic gasification of char from co-pyrolysis of coal and biomass, Fuel Process. Technol. 89 (2008) 890–896, https://doi.org/10.1016/J.FUPROC.2008.03.001.

[40] C.R. Correa, M. Stollovsky, T. Hehr, Y. Rauscher, B. Rolli, A. Kruse, Influence of the carbonization process on activated carbon properties from lignin and lignin-rich biomasses, ACS Sustain. Chem. Eng. 5 (2017) 8222–8233, https://doi.org/10.1021/acssuschemeng.7b01895.

[41] C. Di Stasi, G. Greco, R.L.S. Canevesi, M.T. Izquierdo, V. Fierro, A. Celzard, B. González, J.J. Manyà, Influence of activation conditions on textural properties and performance of activated biochars for pyrolysis vapors upgrading, Fuel 289 (2021), 119759, https://doi.org/10.1016/j.fuel.2020.119759.

[42] C. Di Blasi, G. Signorelli, C. Di Russo, G. Rea, Product distribution from pyrolysis of wood and agricultural residues, Ind. Eng. Chem. Res. 38 (1999) 2216–2224, https://doi.org/10.1021/ie980711u.

[43] A.V. McBeath, C.M. Wurster, M.I. Bird, Influence of feedstock properties and pyrolysis conditions on biochar carbon stability as determined by hydrogen pyrolysis, Biomass Bioenergy 73 (2015), https://doi.org/10.1016/j.biombioe.2014.12.022.

[44] E. Buss, Gravimetric measurement of binary gas adsorption equilibria of methane—carbon dioxide mixtures on activated carbon, Gas Separ. Purif. 9 (1995) 189–197, https://doi.org/10.1016/0950-4214(95)98226-B.

[45] S. Furmaniak, P. Kowalczyk, A.P. Terzyk, P.A. Gauden, P.J.F. Harris, Synergetic effect of carbon nanopore size and surface oxidation on CO2 capture from CO2/CH4 mixtures, J. Colloid Interface Sci. 397 (2013) 144–153, https://doi.org/10.1016/j.jcis.2013.01.044.

[46] R.L.S. Canevesi, S. Schaefer, M.T. Izquierdo, A. Celzard, V. Fierro, Roles of surface chemistry and texture of nanoporous activated carbons in CO2 capture, ACS Appl. Nano Mater. (2022), https://doi.org/10.1021/acsanm.1c04474.

[47] Brascarbo agroindustrial Ltda., n.d. https://brascarbo.com.br/carvao/. (Accessed 15 March 2022).